Spin effects in empty electronic states of Ni(001)

1992 J. Phys.: Condens. Matter 4 4293

(http://iopscience.iop.org/0953-8984/4/17/008)

J. Phys.: Condens. Matter 4 (1992) 4293–4300. Printed in the UK

Spin effects in empty electronic states of Ni(001)

R Schneider†, K Starke†§, K Ertl†, M Donath†, V Dose†, J Braun‡, M Graß‡ and G Borstel‡

† Max-Planck-Institut für Plasmaphysik, Euratom-Association, W-8046 Garching bei München, Federal Republic of Germany

‡ Fachbereich Physik, Universität Osnabrück, W-4500 Osnabrück, Federal Republic of Germany

Received 12 December 1991

Abstract. In this paper spin-dependent calculations within the one-step model of inverse photoemission are presented for the Ni(001) surface. They are compared with spin-resolved inverse photoemission and target current spectroscopy data and are used to construct an effective surface barrier potential. The measured exchange splitting of the X_1 point about 9 eV above the Fermi level as well as dispersions $E(k_\parallel)$ and splittings of bulk and surface states are shown to be well described by the calculations.

1. Introduction

The electronic structure at the surfaces of metals has been studied extensively during recent years. The agreement between experimentally measured dispersion relations $E(k)$ for bulk and surface derived states and *ab initio* calculations was found to be very good, especially for copper which is the most comprehensively investigated system [1, 2]. Since spin polarization has become an additional experimental parameter by preparing a spin-polarized electron beam or analysing the spin polarization of the emitted electrons the study of spin effects has opened up a new and rapidly growing research area. Spin-resolved photoemission (PES) and inverse photoemission (IPE) are able to measure the majority and minority bands of ferromagnets separately [3–6]. Temperature-dependent changes in the spin-split electronic structure have been investigated and compared with theoretical predictions [7–13]. In this paper we will discuss spin effects in the unoccupied electronic structure of Ni(001). Calculations within the one-step model of IPE will be compared with spin-resolved IPE and target current spectroscopy data. As a result of this comparison a realistic effective surface barrier potential will be given.

2. Method

In the one-step model the spectra are calculated within a formalism of independent quasiparticles with finite lifetimes in a semi-infinite crystal by a multiple scattering approach based on the well-known LEED (low-energy electron diffraction) theory. Inside

§ Now at: Institut für Experimentalphysik, Freie Universität Berlin, Arnimallee 14, W-1000 Berlin 33, Federal Republic of Germany.

0953-8984/92/174293+08$04.50

the solid the crystal is modelled by effective one-particle bulk muffin-tin potentials at the positions of the atoms with a real part which is the sum of the Coulomb potential due to the interaction of all charges in the system and the exchange-correlation potential calculated in a local approximation in the density functional theory accounting for many-body effects [14]. The imaginary part of the muffin-tin potential is determined by the imaginary part of the exchange-correlation potential which accounts for inelastic processes resulting in a finite lifetime for the bulk states. The effective potential in front of the surface is chosen as proposed by Rundgren and Malmström [15]: the image potential $1/[4(z - z_{im})]$ at the position z_{im} of the image plane resulting from the attractive force between the image charge inside the metal and the electron in front of the surface is joined to the muffin-tin zero inside the crystal by a third-order polynomial. The height of the surface barrier is determined by the sum of the Fermi energy relative to the muffin-tin zero as given by the band-structure calculation and the measured work function. The surface states can be calculated and the parameters of the barrier potential can be determined by comparing the theoretical results with the measured data. A similar analysis has been carried out for Cu(001) [16].

In the case of one-step model calculations for ferromagnetic materials the two spin systems are treated as separate systems with different effective bulk muffin-tin potentials, but with the same Fermi energy. The surface potential for Ni(001) is modelled in our calculation by the same potential for both spin systems, therefore neglecting the spin dependence of the surface barrier potential itself due to exchange-correlation processes near the crystal surface as shown by jellium calculations for a spin-polarized infinite electron gas. This spin-dependent correction of the surface potential is of the order of $1/(z - z_{im})^2$ [17]. For Ni(001) the discussion of spin-dependent corrections for the surface potential appeared to be unnecessary because of the size of the experimental error bars for the measured peak positions and spin splittings. The state-of-the-art experimental accuracy does not allow the extraction of these spin-dependent corrections by comparing the theoretical and measured data. As a consequence, the calculations are done with a non-spin-dependent surface barrier potential and, therefore, give only the lower limits to the spin splitting of the surface states. All theoretical results will be presented without accounting for any experimental broadening. The calculations are done for zero temperature and therefore assume saturation magnetization.

The experimental data, however, have been taken at temperatures between 540 and 340 K during slow cooling of the sample, i.e. T/T_C was between 0.85 and 0.54 [18]. Consequently, the bulk magnetization of the sample was reduced by between 34 and 11% compared with the saturation value at $T = 0$. The data had to be taken at elevated temperature in order to have a high surface magnetization in remanence. Measurements with the magneto-optic Kerr effect and spin-resolved IPE have shown that the surface magnetization of the investigated Ni(001) surface follows the bulk magnetization only for temperatures above about 400 K. Below 400 K the magneto-crystalline anisotropy favouring the ⟨111⟩ directions as axes of easy magnetization is large enough to destroy the one-domain magnetic state. As a consequence a complicated closure domain structure appears with reduced in-plane magnetization as observed by Kerr microscopy. Therefore the experimental data have been obtained at elevated temperature from a sample in a defined magnetic state but with a surface magnetization reduced by estimated 20% compared with the bulk magnetization at $T = 0$. The apparatus used to obtain the experimental data has been described in the literature [19, 20]. Comprehensive information on the data obtained for Ni(001)

has been published elsewhere [18].

3. Spin effects in target current spectra

A simple experiment to detect spin effects in the unoccupied states is the measurement of the target current I as a function of the energy E of the incoming electrons for spin parallel or anti-parallel to the magnetization direction of the sample. Figure 1 shows the target current for normal electron incidence on Ni(001) for the two spin systems. For energies between 4 and 6 eV above the vacuum level the target current differs depending on the spin polarization of the incoming electrons. Below about 4 eV the target current is reduced by an increased crystal reflectivity due to the $X_{4'}$–X_1 band gap. At the upper band edge X_1 at about 5 eV above the vacuum energy the target current increases because the electrons can penetrate with higher probability into the crystal. X_1 is located about 200 meV higher for the minority compared with the majority spin system. This is a result of the hybridization of the magnetic d bands with the sp bands that form the boundaries of the gap. In nickel the uppermost half-filled d band is responsible for the ferromagnetism. The other d bands as well as sp bands are polarized by it.

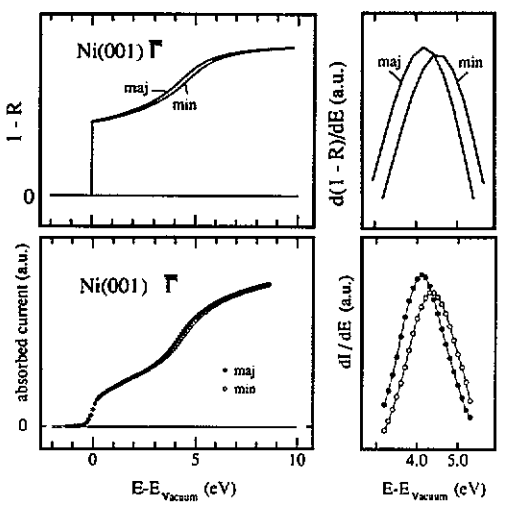

Figure 1. Spin-resolved target current spectra $I(E)$ and their derivative dI/dE for normal electron incidence on Ni(001) (lower part) in comparison with calculated transmission data $1 - R(E)$ and their derivative (upper part).

Comparison of the measured target current with the calculated transmission coefficients for both spin systems may test the quality of the effective one-particle muffin-tin potentials of Moruzzi *et al* [14]. The energy dependence of the transmission coefficient is calculated as $1 - R(E)$, where $R(E)$ is the elastic reflection coefficient. It can be calculated within the LEED multiple scattering formalism of the one-step model as the sum of the intensities of the LEED beams leaving the surface at energy E. We neglect the contribution of inelastic reflection which is known to be a comparatively slowly varying function of E. In the calculation the imaginary part of the muffin-tin potential was chosen as -0.05 eV. The calculated transmission agrees well with the measured target current (figure 1). The spin splitting in figure 1 and the spin asymmetry $(I_\uparrow - I_\downarrow)/(I_\uparrow + I_\downarrow)$ in figure 2 are also well reproduced by the calculations, indicating the good quality of the muffin-tin potentials.

We want to note that the spin asymmetry of the target current due to a spin-split band edge can be used as a convenient spin polarization detector [21].

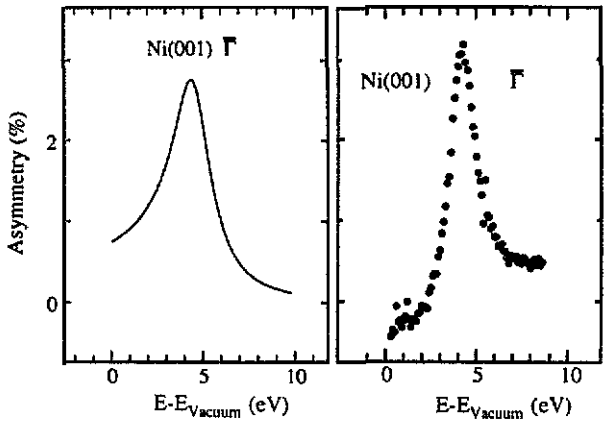

Figure 2. Calculated (left panel) and measured (right panel) spin asymmetry for the data shown in figure 1.

4. Spin effects in inverse photoemission spectra

In this section we will compare the dispersion and the spin splittings of empty bulk and surface derived states of Ni(001) with one-step model calculations. The IPE spectra for a photon energy of 9.4 eV are calculated within the one-step model using muffin-tin potentials described in section 2. Thörner and Borstel [22] have already calculated the spin-integrated IPE spectra of Ni(001) with a step barrier. They were able to describe bulk-derived features in spectra obtained by IPE [23]. We have done similar calculations, but spin-dependent and using a more realistic surface barrier as described above [15], as shown in figure 3. The surface barrier height is given as the sum of the Fermi energy relative to the muffin-tin zero (9.29 eV) and the measured work function (5.30 eV) to 14.59 eV. We compare our calculations with the latest spin-resolved data obtained for Ni(001) [18]. Earlier spin-integrated data [23, 24] exhibit somewhat different dispersion relations $E(k_{\|})$. We want to emphasize that our new experimental setup provides improved k resolution. This has been made possible by using a more sophisticated electron optics, careful magnetic shielding and eliminating any magnetic material close to the sample [19, 20].

The calculation gives a good reproduction of the measured dispersions of bulk and surface states as shown in figure 4. Due to the limited energy resolution in IPE, however, the surface barrier cannot be reconstructed with high accuracy from IPE data alone. The two quite different surface potentials ($z_{im} = -1.0$ Å for a and -0.5 Å for b) shown in figure 3 are both able to describe the measured surface state dispersions and spin splittings within the experimental errors. The IPE data for the crystal-induced surface state around $\overline{X}$ determine the matching region of the image potential to the bulk muffin-tin zero by the third-order polynomial part of the surface potential. We note here that self-consistent jellium calculations of surface potentials indicate that the position of the image plane for Ni(001) should be very similar to Cu(001). Calculations within the one-step model for Cu(001)

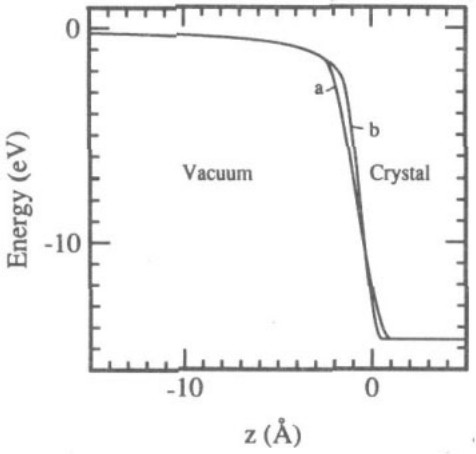

Figure 3. Surface potentials with two different positions for the image plane used for the calculation: $z_{im} = -1.0$ Å for a and -0.5 Å for b. a describes all experimental data well. b was used to demonstrate the sensitivity of the calculations with z_{im}.

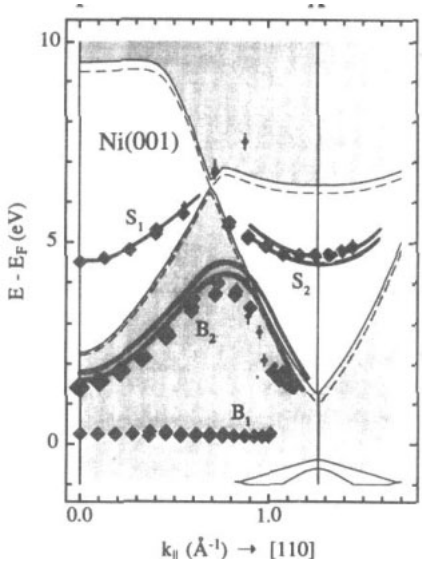

Figure 4. Measured (diamonds, spin-integrated) and calculated (full curves, spin-resolved) band dispersions $E(k_\parallel)$ of empty states on Ni(001).

give $z_{im} = -1.12$ Å [16]. Therefore the surface potential a with $z_{im} = -1.0$ Å seems to be more realistic than b with $z_{im} = -0.5$ Å. To determine the surface barrier more accurately high-resolution two-photon photoemission (2PPE) results for the $n = 1$ image-potential-induced surface state are necessary. 2PPE measurements give a binding energy of 0.61 eV for the $n = 1$ image-potential state [25]. Taking this result into account it is possible to fix the position of the image plane at -1.0 Å, a value also favoured previously.

In table 1 the calculated spin-dependent final energies E_f above E_F are shown together with their splitting Δ of bulk and surface states on Ni(001) for the two surface potentials a and b. For the transition between sp bands B_2 for normal electron incidence the calculation gives a splitting of about 190 meV compared with the experimental value of only 80 ± 20 meV. The discrepancy cannot only be explained by the reduced saturation magnetization in the experiment. More likely it is caused by an inadequate treatment of electron correlations in the calculation. It is well known that the theoretical values for exchange splittings of the d bands in nickel are larger than the experimental ones by a factor of two or three unless 3d electron correlation effects are taken into account in a proper way [9–11]. Table 1 shows that the sp transition B_2 (especially for normal electron incidence) has some 'surface contribution' because it is slightly affected by the different surface barriers.

The theoretically expected spin effects for the crystal-induced surface state S_2 as well as for the barrier-induced surface state S_1 agree with the measured data within the experimental errors. For S_2 one expects an exchange splitting of about 240 meV

Table 1. Calculated spin-dependent final state energies E_f above the Fermi level and their splitting Δ of the sp-like bulk transition B_2, the barrier-induced surface state S_1 and the crystal-induced surface state S_2 on Ni(001) obtained with two different surface potentials *a* and *b* as shown in figure 3.

		Potential			
θ (deg)		*a*	*b*	*a*	*b*
		sp-bulk transition B_2		Barrier-induced surface state ($n = 1$) S_1	
	$E_{f,maj}$ (eV)	1.6703	1.6886	4.7036	4.7822
0	$E_{f,min}$ (eV)	1.8641	1.8726	4.7167	4.7885
	Δ (meV)	193.8	184.0	13.1	6.3
		sp-bulk transition B_2		Crystal-induced surface state S_2	
	$E_{f,maj}$ (eV)	3.1282	3.1173	4.6676	4.6752
48	$E_{f,min}$ (eV)	3.3628	3.3522	4.8412	4.8534
	Δ (meV)	234.6	234.9	173.6	178.2
	$E_{f,maj}$ (eV)	2.5116	2.4953	4.5342	4.5270
56	$E_{f,min}$ (eV)	2.7585	2.7414	4.7061	4.7161
	Δ (meV)	246.9	246.1	171.9	189.1

compared with 180 ± 80 meV in experiment, whereas the image state should exhibit a splitting of only about 10 meV. The experimental result of 13 ± 13 meV is compatible with that†. The difference in the expected spin splittings for the two different kind of surface states can be understood in the following way. Barrier-induced surface states like S_1 have wavefunctions with their highest probability some ångstroms in front of the surface in the vacuum region. Consequently they are mostly influenced by the long-range image potential caused by the image charge of the incoming electron giving rise to this Rydberg-like series of states pinned to the vacuum level. The wavefunction and the image potential is expected to be almost insensitive to the shape of the surface potential directly at the surface or in the bulk. Because the image potential is spin independent or at most only weakly spin-dependent (see section 2) the barrier-induced surface states are not expected to exhibit a large exchange splitting. On the contrary, crystal-induced surface states are very sensitive to the potential at the surface, because their wavefunction is mostly concentrated within the first atomic layer. In addition, they are strongly influenced by the bulk electronic structure. Therefore one expects a spin splitting that may reflect the splitting of the bulk bands terminating the band gap. Within the formalism of the phase accumulation or multiple reflection model [26–29] the spin splitting of crystal-induced surface states are mainly determined by the spin-dependent crystal phases shifted for the two spin systems by about 200 meV for the $X_{4'}$–X_1 gap of Ni(001). This results in a spin splitting of the same order for the crystal-induced states. Within this model the barrier-induced surface states are mainly determined by the barrier phase which is spin independent or only weakly spin-dependent because of the surface potential. Therefore in this approach the splitting is also expected to be small consistent with the considerations given earlier.

The measured IPE spectra are well reproduced by the calculations. Examples are shown in figure 5 for B_2 and in figure 6 for S_2. Only the measured minority

† Spin-resolved IPE spectra of the barrier-induced surface state are shown in [18]. The procedure for obtaining this very small splitting of the two spin components from the data is also described there.

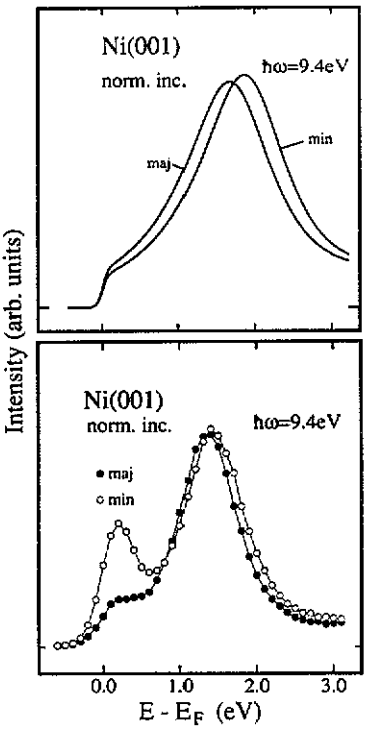

Figure 5. Calculated (upper panel) and measured (lower panel) spin-resolved IPE spectra obtained for Ni(001) displaying the transition between sp-like states B_2.

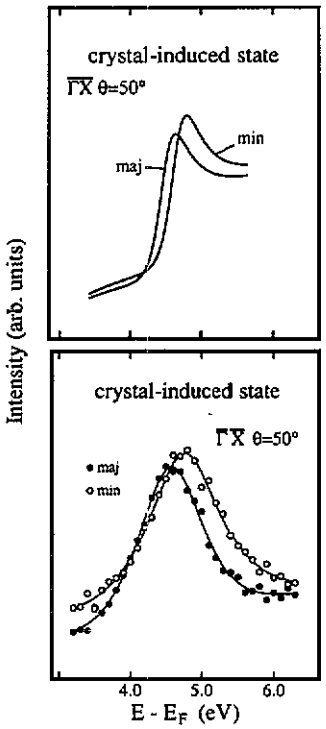

Figure 6. Calculated (upper panel) and measured (lower panel) spin-resolved IPE spectra obtained for Ni(001) displaying the transition into the crystal-induced surface state S_2.

structure close to the Fermi level in figure 5 that is related to transitions into empty minority d states is not reproduced in the calculated spectra. Calculating the direct transitions and their matrix elements with a combined interpolation scheme gives the same result. Therefore we suggest that this structure reflects processes not included in the one-step model, e.g. density of states effects, produced by non-k-conserving transitions into minority d states just above the Fermi level.

Finally, let us describe one more aspect. The one-step calculation even reproduces details of the line shape. The line shape of the transition into the crystal-induced surface state S_2 shown in figure 6 is asymmetric and broader at higher energies. This is a result of the higher de-exitation probability by bulk states the closer one gets to the gap edge. It can be understood in analogy to the increased target current at the gap edge due to the reduced reflectivity outside the gap (see section 3). Furthermore, the minority peak width is slightly larger than the majority one both in experiment and calculation. The shorter lifetime of the spin-down state follows from the high density of minority d holes just above the Fermi level [30].

5. Summary

A comparison of one-step model calculations for Ni(001) with spin-resolved IPE as

well as target current spectroscopy data has been presented. Energy dispersions $E(k_{\parallel})$, spin splittings and even details in the line shape of transitions that are measured via spin-resolved IPE are well described by these calculations. In combination with two-photon photoemission data of the image-potential-induced surface state the shape of the surface potential has been reconstructed. Spin-resolved target current spectroscopy data revealing a 3% spin asymmetry at the upper band gap edge at X_1 are well reproduced by calculations of the elastic reflection coefficient as a function of energy. The results for bulk-derived features indicate that a more sophisticated treatment of electron correlation effects may improve the agreement between experiment and calculations.

Acknowledgment

We thank S Schuppler for making his results available to us prior to publication.

References

[1] Courths R and Hüfner S 1984 *Phys. Rep.* **112** 53
[2] Schneider R, Dürr H, Fauster Th and Dose V 1990 *Phys. Rev.* B **42** 1638
[3] Raue R, Hopster H and Clauberg R 1983 *Phys. Rev. Lett.* **50** 1623
[4] Unguris J, Seiler A, Celotta R J, Pierce D T, Johnson P D and Smith N V 1982 *Phys. Rev. Lett.* **49** 1047
[5] Dose V and Glöbl M 1985 *Polarized Electrons in Surface Physics, Advanced Series in Surface Science* ed R Feder (Singapore: World Scientific) p 547
[6] Donath M 1989 *Appl. Phys.* A **49** 351
[7] Hopster H, Raue R, Güntherodt G, Kisker E, Clauberg R, Campagna M 1983 *Phys. Rev. Lett.* **51** 829
[8] Donath M and Dose V 1989 *Europhys. Lett.* **9** 821
[9] Nolting W, Borgiel W, Dose V and Fauster Th 1989 *Phys. Rev.* B **40** 5015
[10] Borgiel W, Nolting W and Donath M 1989 *Solid State Commun.* **72** 825
[11] Nolting W, Braun J, Borstel G, Borgiel W 1990 *Phys. Scr.* **41** 601
[12] Kämper K P, Schmitt W and Güntherodt G 1990 *Phys. Rev.* B **42** 10696
[13] Braun J, Nolting W and Borstel G 1991 *Surf. Sci.* **251/252** 22
[14] Moruzzi V L, Janak J F, Williams A R 1978 *Calculated Electronic Properties of Metals* (New York: Pergamon)
[15] Rundgren J and Malmström G 1977 *J. Phys. C: Solid State Phys.* **10** 4671
[16] Thörner G and Borstel G 1986 *Appl. Phys.* A **41** 99
[17] Thörner G and Borstel G 1987 *Verhandl. DPG* (VI) **22** O–32
[18] Starke K, Ertl K, Donath M and Dose V 1990 *Vacuum* **41** 755
Starke K, Ertl K and Dose V 1992 *Phys. Rev.* B at press
[19] Kolac U, Donath M, Ertl K, Liebl H and Dose V 1988 *Rev. Sci. Instrum.* **59** 1933
[20] Donath M, Dose V, Ertl K and Kolac U 1990 *Phys. Rev.* B **41** 5509
[21] Tillmann D, Thiel R and Kisker E 1989 *Z. Phys.* B **77** 1
[22] Thörner G and Borstel G 1984 *Solid State Commun.* **49** 997
[23] Desinger K, Dose V, Glöbl M and Scheidt H 1984 *Solid State Commun.* **49** 479
[24] Goldmann A, Donath M, Altmann W and Dose V 1985 *Phys. Rev.* B **32** 837
[25] Schuppler S 1991 *PhD Thesis* Ludwig-Maximilians-Universität München
[26] Echenique P M and Pendry J B 1978 *J. Phys. C: Solid State Phys.* **11** 2065
[27] McRae E G 1979 *Rev. Mod. Phys.* **51** 541
[28] Smith N V 1985 *Phys. Rev.* B **32** 3549
[29] Smith N V and Chen C T 1989 *Phys. Rev.* B **40** 7565
[30] Feder R and Rodriguez A 1984 *Solid State Commun.* **50** 1033